NANO LETTERS

Letter

Cite This: Nano Lett. 2019, 19, 1682−1687

pubs.acs.org/NanoLett

Nanomagnetism of Magnetoelectric Granular Thin-Film Antiferromagnets

Patrick Appel,[†,∥] Brendan J. Shields,[†,∥] Tobias Kosub,[‡,§] Natascha Hedrich,[†] René Hübner,[‡] Jürgen Faßbender,[‡] Denys Makarov,[‡,§] and Patrick Maletinsky*[,†]

[†]Department of Physics, University of Basel, Klingelbergstrasse 82, Basel CH-4056, Switzerland

[‡]Helmholtz-Zentrum Dresden-Rossendorf e.V., Institute of Ion Beam Physics and Materials Research, 01328 Dresden, Germany

[§]Institute for Integrative Nanosciences, Institute for Solid State and Materials Research (IFW Dresden e.V.), 01069 Dresden, Germany

Supporting Information

ABSTRACT: Antiferromagnets have recently emerged as attractive platforms for spintronics applications, offering fundamentally new functionalities compared with their ferromagnetic counterparts. Whereas nanoscale thin-film materials are key to the development of future antiferromagnetic spintronic technologies, existing experimental tools tend to suffer from low resolution or expensive and complex equipment requirements. We offer a simple, high-resolution alternative by addressing the ubiquitous surface magnetization of magnetoelectric antiferromagnets in a granular thin-film sample on the nanoscale using single-spin magnetometry in combination with spin-sensitive transport experiments. Specifically, we quantitatively image the evolution of individual nanoscale antiferromagnetic domains in 200 nm thin films of Cr_2O_3 in real space and across the paramagnet-to-antiferromagnet phase transition, finding an average domain size of 230 nm, several times larger than the average grain size in the film. These experiments allow us to discern key properties of the Cr_2O_3 thin film, including the boundary magnetic moment density, the variation of critical temperature throughout the film, the mechanism of domain formation, and the strength of exchange coupling between individual grains comprising the film. Our work offers novel insights into the magnetic ordering mechanism of Cr_2O_3 and firmly establishes single-spin magnetometry as a versatile and widely applicable tool for addressing antiferromagnetic thin films on the nanoscale.

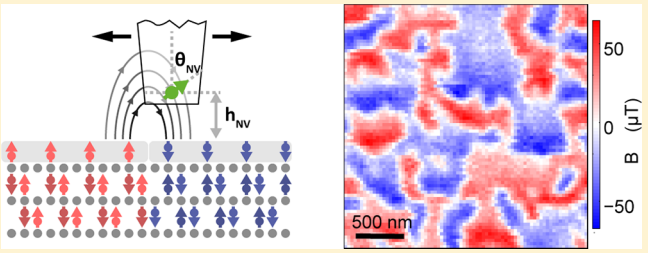

KEYWORDS: *Antiferromagnets, magnetoelectrics, surface magnetization, intergranular exchange energy, nitrogen vacancy magnetometry, Hall magnetometry*

Antiferromagnetic (AF) materials are abundant in nature, much more so than ferromagnets, but have been studied less thoroughly due to their insensitivity to magnetic fields and vanishing magnetization. Still, it has been widely recognized that faster and smaller spintronic devices require the use of purely AF, nanoscale, thin-film systems.[1−8] The properties of such thin films deviate significantly from their bulk parents due to their morphology, which typically consists of closely packed grains. This granularity leads to the appearance of nanoscale domains with strongly pinned domain walls,[6,8−10] a dramatic departure from the bulk case where domains are typically on the millimeter scale.[13] Such behavior cannot be explained by a change of material properties such as magnetic anisotropy and exchange in the bulk volume. Instead, the influence of the surface becomes significant, namely, the boundary magnetism and the intergranular exchange coupling, dramatically changing the behavior of AFs. Imaging of domain structures for thin films is difficult. There exist a few techniques, including X-ray magnetic dichroism photoelectron emission microscopy (XML(C)D PEEM)[11] as well as magnetic force microscopy (MFM),[12] that are able to image thin-film domains, yet real-space imaging of magnetic domain nucleation and its influence on the electron transport response remains largely unexplored for thin-film AFs.

We present a consistent and quantitative study of these properties based on nanoscale nitrogen vacancy (NV) single-spin magnetic imaging[14] and zero-offset anomalous Hall effect magnetometry (ZOHM)[15] for a Cr_2O_3 thin film. This collinear magnetoelectric AF is highly relevant to AF spintronics,[8] making it a showcase example of this combined approach. We image and study the formation of nanoscale domains across the paramagnet−AF phase transition with unprecedented signal-to-noise ratio and sub-100 nm spatial resolution, enabling a quantitative determination of the boundary magnetization. We find an average domain size of 230 nm, several times larger than the grain size of 50 nm in our film, indicating significant

Received: November 20, 2018
Revised: January 28, 2019
Published: January 31, 2019

DOI: 10.1021/acs.nanolett.8b04681
Nano Lett. 2019, 19, 1682−1687

intergranular exchange coupling that dominates the magnetic alignment of neighboring grains. Furthermore, our ZOHM measurements allow us to determine the distribution of critical temperature across the grains of our film, enabling us to model the domain formation process and to confirm the strong intergranular exchange coupling.

Because of its room-temperature ordering and magnetoelectric switching capabilities,[8,16,17] Cr_2O_3 is a key contender for future AF-based magnetoelectric memory devices. Breaking of the crystal bulk symmetry leads to the formation of a (0001) surface that consists of a layer of Cr atoms all belonging to the same AF sublattice. This surface termination presents a roughness-insensitive, out-of-plane surface magnetization on the order of few μ_B/nm^2 (where μ_B is the Bohr magneton) whose orientation is rigidly linked to the AF order parameter[16,18,19] (Figure 1b). Past work has shown that as the temperature approaches the critical temperature (T_{crit}) the magnetization remains out-of-plane and is reduced in amplitude.[20] This surface magnetization creates stray magnetic fields, which, in the far field, are quadrupolar in nature and decay with distance from the sample over length scales given by typical domain sizes or sample thickness.[19,21,22] Exploiting such stray fields to address thin-film samples thus requires a sensitive magnetometer that can be brought in close proximity to the sample.

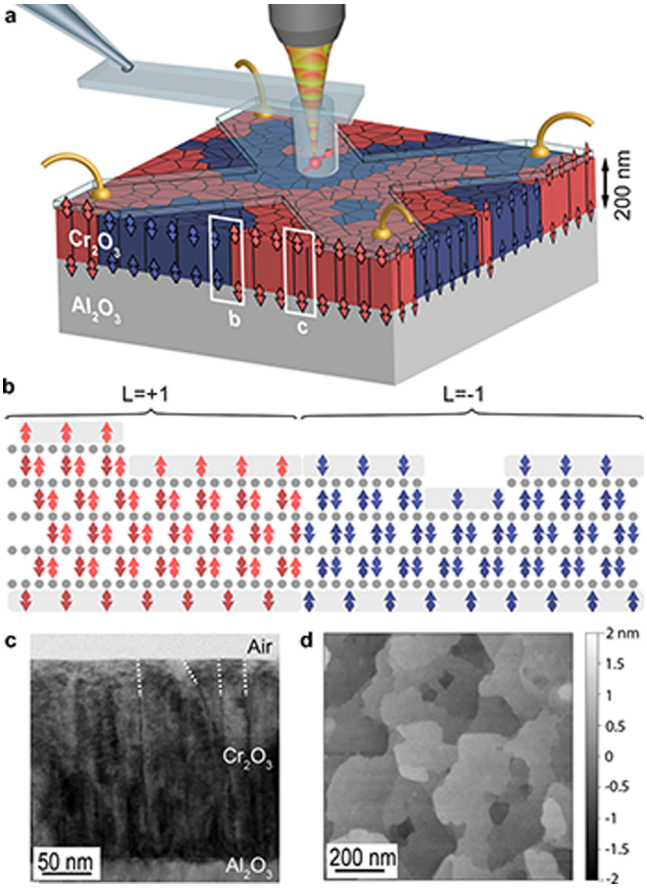

Figure 1. Schematic of experiment and thin-film antiferromagnetic sample. (a) Thin-film sample of antiferromagnetic Cr_2O_3 is examined using a combination of scanning single-spin magnetometry (red arrow) and zero-offset Hall magnetometry (light-blue cross with golden leads). (b) Cr_2O_3 is a bulk antiferromagnet with a roughness-insensitive, nonzero surface magnetization linked to the underlying order parameter, L. (c) Cross-sectional transmission electron microscopy image of the sample. The image shows the typical columnar grains comprising the Cr_2O_3 film (representative grain boundaries are highlighted by white dashed lines). (d) Atomic force microscopy of the Cr_2O_3 sample surface, showing atomically smooth terraces.

This nontrivial requirement is met by nanoscale, scanning NV magnetometry (Figure 1a),[14,23,24] a versatile technique that has previously been used to study magnetism in ferromagnetic films[25] and noncollinear antiferromagnets.[26] The technique operates by scanning a single electronic spin in close vicinity to a surface to measure the magnetic field, B_{NV}, along the fixed NV quantization axis through the Zeeman splitting of the NV's optically detected electron spin resonance (see Supporting Information). It operates under ambient conditions and offers quantitative sensing, nanoscale imaging, and sensitivities sufficient to address individual electronic spins.[27] These unique characteristics are ideally suited to address the nanoscale properties of pure AF systems, which lack an overall magnetic moment.

The samples we investigate consist of 200 nm thick Cr_2O_3 films grown on a c-cut sapphire substrate (see Supporting Information). The obtained film is granular with ~50 nm sized columnar grains (Figure 1c) and very high crystallinity within each grain.[28] The samples exhibit atomically smooth terraces bounded by 0.26 nm steps in topography, corresponding to single Cr−O_3−Cr repetitions, as confirmed by atomic force microscopy (Figure 1d). For NV magnetometry, the sample is mounted on a Peltier element to control temperatures to within ±0.1 K during measurements. We prepare the film by heating it well above the AF-to-paramagnet transition (T_{Neel} = 308 K in bulk[12]) and then cooling it back to the AF state in zero external magnetic field to induce a spontaneously formed pattern of AF domains.[8]

To investigate AF domains in the Cr_2O_3 film, we first use NV magnetometry to acquire a map of B_{NV} at the Cr_2O_3 surface. In contrast with previous measurements of noncollinear AFs, where the measured stray field emerges from an overall ferrimagnetic moment due to the canting of the spins, in Cr_2O_3, NV magnetometry probes the stray field resulting from a single layer of uncompensated spins on the surface. The acquired stray field image then immediately confirms the presence of magnetic domains, as signaled by areas of positive or negative B_{NV}, as shown in Figure 2a. Repeated scans of the same area show the same magnetic field pattern, indicating a minimal effect of the laser and microwave fields on the sample.[28] As expected from a simplified picture of homogeneously magnetized domains with infinitely sharp domain walls,[25] zeros in B_{NV} indicate the locations of domain walls up to a small, constant shift, and broad maxima of B_{NV} occur toward the boundaries of the domains. More quantitatively, we model this stray field by describing the magnetization $\vec{m}$ of the Cr_2O_3 film as two monolayers of out-of-plane polarized spins with moment density $\sigma_z(x, y)$ and opposite orientations, separated by d = 200 nm (Figure 1b): $\vec{m}(x, y, z) = \sigma_z(x, y)[\delta(z) - \delta(z + d)]\hat{z}$, where δ is the Dirac delta function and $\hat{z}$ is the out-of-plane unit vector. The measured stray magnetic field B_{NV} can then be conveniently obtained by established methods of field propagation in Fourier space[29,30]

$$B_{NV}(\vec{k}) = \vec{m}(\vec{k})T_{NV}(h_{NV}, \theta_{NV}, \phi_{NV}, \vec{k}) \quad (1)$$

DOI: 10.1021/acs.nanolett.8b04681
Nano Lett. 2019, 19, 1682−1687

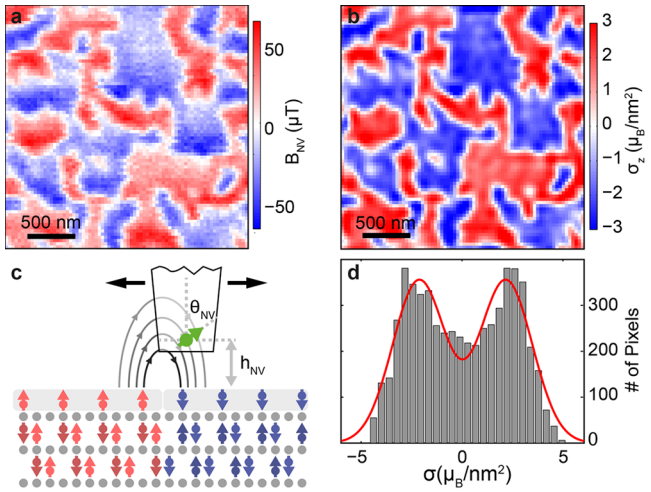

Figure 2. Domain imaging in antiferromagnetic Cr_2O_3. (a) Map of the measured stray magnetic field B_{NV} above the Cr_2O_3 film and (b) the extracted moment density profile (see the main text) of the film, which reveals a domain pattern of spin-up and spin-down domains. (c) Measurement geometry and relevant experimental parameters for reverse propagation. (d) Histogram of surface moment density values found in panel b with a fit to a bimodal, Gaussian distribution (red), yielding an average moment density 2.14 ± 1.5 μ_B/nm^2.

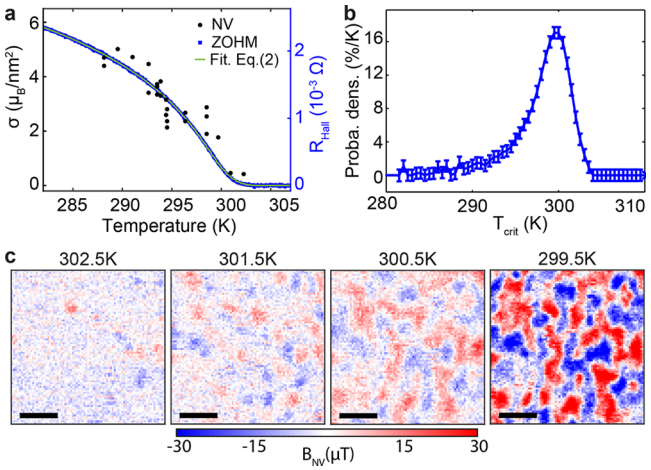

Figure 3. Spatial variation of critical temperatures. (a) Temperature dependence of moment density together with ZOHM data.[15] The data are fitted (green) to a critical behavior with spatially varying critical temperatures (see eq 2 and the text for details). (b) Probability distribution of critical temperatures as determined from the fit in panel a. (c) Consecutive magnetic field maps obtained during cooling of the sample through the phase transition. Domains are nucleating at isolated spots and propagate laterally to form the domain pattern (scale bar: 500 nm).

where T_{NV} is a propagator that depends on the NV orientation (θ_{NV}, ϕ_{NV}) and the NV-to-sample distance, h_{NV} (see Figure 2c). If h_{NV}, θ_{NV}, and ϕ_{NV} are known, then eq 1 can be inverted and $\sigma_z(x, y)$ directly obtained from the experimental data together with appropriate filtering.[29] To determine these parameters, we developed an iterative, self-consistent method based on the data and our minimal model for Cr_2O_3's surface magnetization described above. Using the resulting values h_{NV} = 120 nm, θ_{NV} = 54°, and ϕ_{NV} = 92°, we reverse propagate the measured $B_{NV}(x, y)$ map to find $\sigma_z(x, y)$, as shown in Figure 2b. This magnetization profile shows well-defined magnetic domains, with typical domain sizes ∼230 nm (determined by the peak width of the corresponding autocorrelation map), significantly larger than the 50 nm grain size in our film, indicating an intergranular exchange coupling that influences the order-parameter alignment of neighboring grains. At the same time, the very existence of domains and the small domain-wall feature size (on the scale of the grain size) suggest that strong pinning occurs at the grain boundaries during the cooling process. The reverse propagation also yields the average surface moment density of 2.14 ± 1.5 μ_B/nm^2, as determined from a histogram of the inferred moment density map (Figure 2d). This represents the first measurement of the boundary magnetization of Cr_2O_3 at room temperature and is independently confirmed through additional measurements on a patterned thin-film Cr_2O_3 sample, which we prepared in a monodomain state by field cooling and on a patterned bulk, monodomain, single-crystal sample.[28]

Further details of the nanoscale magnetic properties of our thin-film AF can be obtained by observing the temperature dependence of σ_z near the AF−paramagnet transition at the critical temperature of the thin film. We thus repeated moment density measurements for temperatures around T_{Neel} and compared our findings to ZOHM measurements performed on a similarly prepared sample[15] (Figure 3a). In brief, ZOHM measures the anomalous Hall resistance in a thin layer of Pt evaporated onto the Cr_2O_3 surface and is sensitive to the average Cr_2O_3 surface magnetic moment over the Hall cross area of ∼900 μm^2. This method gives a precise readout of the averaged relative magnetization but does not provide spatial resolution or the magnitude of the moment density. The NV magnetometry data (Figure 3a) follow the temperature dependence of ZOHM and thereby allow us to calibrate the resulting Hall resistance to a quantitative magnetic moment density.

The temperature dependence of σ_z determined by combining ZOHM and NV magnetometry (Figure 3a) shows a smooth tapering of σ_z through the phase transition, in contrast with the sharp drop to zero expected from the usually observed power-law dependence of $\sigma(T)$ for magnetic phase transitions. Such behavior was previously attributed to spatial variations of T_{crit} in thin films[31,32] and can be readily accounted for by the convolution

$$\sigma_{avg}(T) = \int P(T_{crit})\sigma\left(\frac{T}{T_{crit}}\right) dT_{crit} \quad (2)$$

where $P(T_{crit})$ is the probability density for T_{crit} and $\sigma(\tau) = \sigma_{sat}(1 - \tau)^{\beta}$, with critical exponent, β, and saturation magnetization, σ_{sat} ($\sigma(\tau > 1) = 0$). Fitting eq 2 to our data (green curve in Figure 3a) for fixed β = 0.35 allows us to extract $P(T_{crit})$, as depicted in Figure 3b. The significant broadening of $P(T_{crit})$ is evidence of the local inhomogeneity of T_{crit} in the sample, which we assign to material defects such as twinning boundaries or lattice dislocations.[8]

The ability to measure fine spatial features of the magnetization pattern enables a detailed study of the paramagnetic-to-AF phase transition and the local variations in T_{crit} at the level of individual domains. To directly observe these variations, we record snapshots of the stray field around T_{crit} (Figure 3c). For the sample well above T_{crit}, we detect no magnetic stray field exceeding our measurement noise, which indicates no surface magnetization and a paramagnetic phase. As the sample is cooled, spatially separated regions of nonzero

DOI: 10.1021/acs.nanolett.8b04681
Nano Lett. 2019, 19, 1682−1687

magnetization spontaneously nucleate, but significant areas of the sample remain paramagnetic. Upon further cooling, this nucleation propagates until all areas of the sample show nonzero magnetization. This lateral spreading of AF domains with decreasing temperature is indicative of significant, intergranular exchange coupling. Without such coupling, each grain would nucleate independently and in a random fashion so that domains would typically be on the order of the grain size.

We developed a discrete model of the AF film[28] based on our observations, taking into account inhomogeneities in T_{crit} and the order parameter, σ_z. The discrete grains comprising the film are mutually exchange-coupled with a probability, P_E, for the order parameter of neighboring grains to be locked by exchange (i.e., for exchange coupling exceeding thermal fluctuations). To test this interpretation, we also developed a differential field cooling (DFC) method (Figure 4a), which

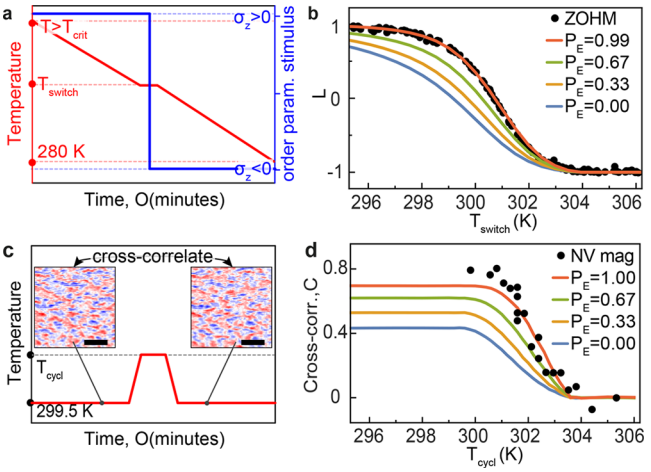

Figure 4. Determining intergranular exchange coupling. (a) Procedure for differential field cooling. The sample was cooled from a temperature $T > T_{crit}$ to $T = T_{switch}$ while applying a strong order-parameter selection stimulus (magnetic field) toward $\sigma_z > 0$. The stimulus was then inverted toward $\sigma_z < 0$, and the sample was further cooled to 280 K. (b) Average order parameter $L = \langle\sigma_z(T_{switch})\rangle/\langle\sigma_z(T_{RT})\rangle$, measured by ZOHM, as a function of T_{switch}. Data are fit to theory (see the text) using the probability distribution from Figure 3b and demonstrate significant intergranular exchange coupling $P_E \approx 1$. (c) Procedure for temperature cycling domain cross-correlation. The sample is imaged at $T_{start} = 299.5$ K, subsequently heated to $T = T_{cycl}$, and cooled back to T_{start}, where another image is taken (scale bar: 1 μm). (d) Cross-correlation between reference and sample image as a function of T_{cycl}, evidencing strong intergranular exchange coupling on the nanoscale.

allows us to assess the efficiency of intergranular exchange coupling through ZOHM.[33] We initialized the sample well above T_{crit} and then applied a strong magnetic field in the $+\hat{z}$ direction to provide an order-parameter selection stimulus[8] toward an AF state with $\sigma_z > 0$ while the sample is cooled. At a temperature T_{switch}, the magnetic field is reversed to yield a stimulus toward $\sigma_z < 0$, with which the sample is further cooled to 280 K. Finally, we measure the average order parameter $\langle\sigma_z(T_{switch})\rangle$ using ZOHM and determine the normalized magnetization $L = \langle\sigma_z(T_{switch})\rangle/\langle\sigma_z(T_{RT})\rangle$ as a function of T_{switch} (Figure 4b). We can use our model to understand the evolutions of L. For $P_E = 0$, grains are independent, and their value of σ_z is determined by an applied order-parameter selection stimulus at the time of ordering, hence, $L(T_{switch}) = -1 + 2A(T_{switch})$, where $A(T_{switch}) = \int_{T_{switch}}^{\infty} P(T_{crit})\, dT_{crit}$ is the unitless fractional sample area having $T_{crit} > T_{switch}$. For $P_E > 0$, however, each grain will be influenced by its neighbors and we find $L(T_{switch}, P_E) = -1 + 2A(T_{switch})e^{P_E\cdot(1-A(T_{switch}))}$.[28] A fit of $L(T_{switch}, P_E)$ to the ZOHM data (Figure 4b) thus allows us to determine $P_E = 0.99$, indicating that for our thin-film sample, intergranular exchange coupling largely dominates thermal fluctuations.

Scanning NV magnetometry can also be used to quantitatively confirm such strong exchange coupling of neighboring grains on the level of individual AF domains. For this, we perform domain cross-correlation measurements under temperature cycling (Figure 4c). We record an AF domain image at an initial temperature $T_{start} = 299.5$ K, subsequently set the sample temperature to T_{cycl} for ~10 min, and finally cool the sample back to T_{start}, where we record a second domain image. Specifically, the pixel-by-pixel correlation $C(T_{cycl})$ between reference and sample images (Figure 4d) measures the extent to which the domain pattern is preserved during heating. This procedure yields information closely related to DFC, all while avoiding experimental difficulties of applying and switching strong order-parameter stimuli (i.e., magnetic fields) in our imaging experiment. By analogy to DFC, we expect the correlation between grains to follow $A(T_{cycl})$ for $P_E = 0$, whereas for $P_E > 0$, we expect the domain pattern to be largely determined by high-T_{crit} grains and the transition from correlated to uncorrelated to therefore be pushed to higher temperatures, as confirmed by granular thin-film simulations.[28] A comparison of our correlation data (Figure 4d, black points) to the simulation (solid lines) provides further proof of the strong intergranular exchange coupling, which we obtain on the level of individual domains.

In this work, we have shown that the domain structure of thin-film AFs is largely determined by intergranular exchange coupling, without which domains would be limited to the size of individual grains. We have directly observed the nucleation process of the AF phase by real-space imaging and quantified important material properties of the film including the boundary magnetization and domain size. Furthermore, we correlated the emergent magnetotransport responses with the imaged AF domain pattern. Our results thus constitute an important step toward the general understanding of surface magnetization and domain formation in AFs as well as the appearance of magnetoelectricity in some families of insulating AFs, where confirmation of theories of monopolization strongly relies on the availability of reliable experimental data on boundary magnetization.[34,35] These results are enabled by our versatile method for quantitative nanoscale imaging of AF order in thin-film materials, which uniquely combines two very different but equally powerful techniques: NV magnetometry and ZOHM. Our approach is largely complementary to the existing toolset for studying AF order, such as neutron[36−38] or X-ray[39−43] scattering as well as optical[44] or scanning probe imaging,[12] where combining high spatial resolution with high signal-to-noise ratio and quantitative imaging has remained elusive thus far. Although we have focused on Cr_2O_3, it is important to note that our approach is much more generally applicable. Previous studies using NV magnetometry have been successful in imaging noncollinear AFs[26] that exhibit a ferrimagnetic moment, and here we have shown that also collinear, magnetoelectric AFs that exhibit boundary magnet-

DOI: 10.1021/acs.nanolett.8b04681
Nano Lett. 2019, 19, 1682−1687

ization due to inversion symmetry breaking at the surface[19,21] can be imaged. Furthermore, NV magnetometry is not limited to out-of-plane magnetization but is also sensitive to magnetic fields originating from in-plane moments. Thus NV magnetometry is applicable to a wide range of AFs as long as the resulting surface spin densities are within the NV magnetometry sensitivity limit, making it a valuable tool for nanoscale AF spintronics.

■ ASSOCIATED CONTENT

Supporting Information

The Supporting Information is available free of charge on the ACS Publications website at DOI: 10.1021/acs.nanolett.8b04681.

Detailed method description for NV magnetometry and ZOHM, supporting experimental results, discussion of Cr_2O_3 surface termination, discussion of magnetic moment density determination, theoretical modeling of critical temperatures and granular ordering dynamics, and additional figures (ZIP)

■ AUTHOR INFORMATION

Corresponding Author

*E-mail: patrick.maletinsky@unibas.ch.

ORCID

Natascha Hedrich: 0000-0002-8742-5567

Denys Makarov: 0000-0002-7177-4308

Author Contributions

‖P.A. and B.J.S. contributed equally.

Notes

The authors declare no competing financial interest.

■ ACKNOWLEDGMENTS

We thank Prof. O. G. Schmidt (IFW Dresden) for his insightful input in the initial stage of the project and S. Hoffman (Basel) and V. Jacques (CNRS Montpellier) for helpful discussions. We gratefully acknowledge financial support through the NCCR QSIT, a competence centre funded by the Swiss NSF, the SNI, and through SNF grant no. 143697 and 155845. This research has been partially funded by the European Commission's 7th Framework Program (FP7/2007-2013) under grant agreement number 611143 (DIADEMS), the ERC within the EU Seventh Framework Programme (ERC grant no. 306277), and the EU FET Programme (FET open grant no. 618083).

■ REFERENCES

(1) Sander, D.; Valenzuela, S. O.; Makarov, D.; Marrows, C. H.; Fullerton, E. E.; Fischer, P.; McCord, J.; Vavassori, P.; Mangin, S.; Pirro, P.; et al. The 2017 Magnetism Roadmap. *J. Phys. D: Appl. Phys.* **2017**, *50*, 363001.

(2) Heron, J. T.; Bosse, J. L.; He, Q.; Gao, Y.; Trassin, M.; Ye, L.; Clarkson, J. D.; Wang, C.; Liu, J.; Salahuddin, S.; Ralph, D. C.; Schlom, D. G.; Iniguez, J.; Huey, B. D.; Ramesh, R. Deterministic switching of ferromagnetism at room temperature using an electric field. *Nature* **2014**, *516*, 370−373.

(3) Jungwirth, T.; Marti, X.; Wadley, P.; Wunderlich, J. Antiferromagnetic spintronics. *Nat. Nanotechnol.* **2016**, *11*, 231−41.

(4) Baltz, V.; Manchon, A.; Tsoi, M.; Moriyama, T.; Ono, T.; Tserkovnyak, Y. Antiferromagnetic spintronics. *Rev. Mod. Phys.* **2018**, *90*, No. 015005.

(5) Seki, S.; Ideue, T.; Kubota, M.; Kozuka, Y.; Takagi, R.; Nakamura, M.; Kaneko, Y.; Kawasaki, M.; Tokura, Y. Thermal Generation of Spin Current in an Antiferromagnet. *Phys. Rev. Lett.* **2015**, *115*, 266601.

(6) Wadley, P.; Howells, B.; Železnỳ, J.; Andrews, C.; Hills, V.; Campion, R. P.; Novak, V.; Olejník, K.; Maccherozzi, F.; Dhesi, S.; Martin, S. Y.; Wagner, T.; Wunderlich, J.; Freimuth, F.; Mokrousov, Y.; Kuneš, J.; Chauhan, J. S.; Grzybowski, M. J.; Rushforth, A. W.; Edmonds, K. W.; Gallagher, B. L.; Jungwirth, T. Electrical switching of an antiferromagnet. *Science* **2016**, *351*, 587−590.

(7) Loth, S.; Baumann, S.; Lutz, C. P.; Eigler, D. M.; Heinrich, A. J. Bistability in atomic-scale antiferromagnets. *Science* **2012**, *335*, 196−199.

(8) Kosub, T.; Kopte, M.; Hühne, R.; Appel, P.; Shields, B.; Maletinsky, P.; Hübner, R.; Liedke, M. O.; Fassbender, J.; Schmidt, O. G.; Makarov, D. Purely antiferromagnetic magnetoelectric random access memory. *Nat. Commun.* **2017**, *8*, 13985.

(9) Meinert, M.; Graulich, D.; Matalla-Wagner, T. Electrical Switching of Antiferromagnetic Mn_2Au and the Role of Thermal Activation. *Phys. Rev. Appl.* **2018**, *9*, No. 064040.

(10) O'Grady, K.; Fernandez-Outon, L. E.; Vallejo-Fernandez, G. A new paradigm for exchange bias in polycrystalline thin films. *J. Magn. Magn. Mater.* **2010**, *322*, 883−899.

(11) Grzybowski, M. J.; Wadley, P.; Edmonds, K. W.; Beardsley, R.; Hills, V.; Campion, R. P.; Gallagher, B. L.; Chauhan, J. S.; Novak, V.; Jungwirth, T.; Maccherozzi, F.; Dhesi, S. S. Imaging current-induced switching of antiferromagnetic domains in CuMnAs. *Phys. Rev. Lett.* **2017**, *118*, No. 057701.

(12) Wu, N.; He, X.; Wysocki, A. L.; Lanke, U.; Komesu, T.; Belashchenko, K. D.; Binek, C.; Dowben, P. A. Imaging and Control of Surface Magnetization Domains in a Magnetoelectric Antiferromagnet. *Phys. Rev. Lett.* **2011**, *106*, No. 087202.

(13) Fiebig, M.; Fröhlich, D.; Sluyterman v. L., G.; Pisarev, R. V. Domain topography of antiferromagnetic Cr2O3 by second-harmonic generation. *Appl. Phys. Lett.* **1995**, *66*, 2906−2908.

(14) Maletinsky, P.; Hong, S.; Grinolds, M. S.; Hausmann, B.; Lukin, M. D.; Walsworth, R. L.; Loncar, M.; Yacoby, A. A robust scanning diamond sensor for nanoscale imaging with single nitrogen-vacancy centres. *Nat. Nanotechnol.* **2012**, *7*, 320−324.

(15) Kosub, T.; Kopte, M.; Radu, F.; Schmidt, O. G.; Makarov, D. All-Electric Access to the Magnetic-Field-Invariant Magnetization of Antiferromagnets. *Phys. Rev. Lett.* **2015**, *115*, No. 097201.

(16) He, X.; Wang, Y.; Wu, N.; Caruso, A. N.; Vescovo, E.; Belashchenko, K. D.; Dowben, P. A.; Binek, C. Robust isothermal electric control of exchange bias at room temperature. *Nat. Mater.* **2010**, *9*, 579−585.

(17) Ashida, T.; Oida, M.; Shimomura, N.; Nozaki, T.; Shibata, T.; Sahashi, M. Observation of magnetoelectric effect in Cr2O3/Pt/Co thin film system. *Appl. Phys. Lett.* **2014**, *104*, 152409.

(18) Belashchenko, K. D. Equilibrium Magnetization at the Boundary of a Magnetoelectric Antiferromagnet. *Phys. Rev. Lett.* **2010**, *105*, 147204.

(19) Andreev, A. F. Macroscopic magnetic fields of antiferromagnets. *JETP Lett.* **1996**, *63*, 758−762.

(20) Fallarino, L.; Berger, A.; Binek, C. Giant temperature dependence of the spin reversal field in magnetoelectric chromia. *Appl. Phys. Lett.* **2014**, *104*, No. 022403.

(21) Dzyaloshinskii, I. External magnetic fields of antiferromagnets. *Solid State Commun.* **1992**, *82*, 579−580.

(22) Astrov, D. N.; Ermakov, N. B.; Borovik-Romanov, A. S.; Kolevatov, E. G.; Nizhankovskii, V. I. External quadrupole magnetic field of antiferromagnetic Cr2O3. *JETP Lett.* **1996**, *63*, 745−751.

(23) Appel, P.; Neu, E.; Ganzhorn, M.; Barfuss, A.; Batzer, M.; Gratz, M.; Tschöpe, A.; Maletinsky, P. Fabrication of all diamond scanning probes for nanoscale magnetometry. *Rev. Sci. Instrum.* **2016**, *87*, No. 063703.

(24) Rondin, L.; Tetienne, J.-P.; Hingant, T.; Roch, J.-F.; Maletinsky, P.; Jacques, V. Magnetometry with nitrogen-vacancy defects in diamond. *Rep. Prog. Phys.* **2014**, *77*, 056503.

DOI: 10.1021/acs.nanolett.8b04681
Nano Lett. 2019, 19, 1682−1687

(25) Tetienne, J.-P.; Hingant, T.; Martinez, L.; Rohart, S.; Thiaville, A.; Diez, L. H.; Garcia, K.; Adam, J.-P.; Kim, J.-V.; Roch, J.-F.; Miron, I. M.; Gaudin, G.; Vila, L.; Ocker, B.; Ravelosona, D.; Jacques, V. The nature of domain walls in ultrathin ferromagnets revealed by scanning nanomagnetometry. *Nat. Commun.* **2015**, *6*, 6733.
(26) Gross, I.; Akhtar, W.; Garcia, V.; Martínez, J.; Chouaieb, S.; Garcia, K.; Carrétéro, C.; Barthélémy, A.; Appel, P.; Maletinsky, P.; Kim, J.-V.; Chauleau, J. Y.; Jaouen, N.; Viret, M.; Bibes, M.; Fusil, S.; Jacques, V. Real-space imaging of non-collinear antiferromagnetic order with a single-spin magnetometer. *Nature* **2017**, *549*, 252−256.
(27) Grinolds, M. S.; Hong, S.; Maletinsky, P.; Luan, L.; Lukin, M. D.; Walsworth, R. L.; Yacoby, A. Nanoscale magnetic imaging of a single electron spin under ambient conditions. *Nat. Phys.* **2013**, *9*, 215−219.
(28) See the Supporting Information for information regarding the implementation of NV magnetometry and ZOHM, sample preparation, a detailed description of the determination of the magnetic moment density, determination of $P(T_{crit})$, and modeling of granular ordering dynamics in the film.
(29) Meyer, E.; Hug, H. J.; Bennewitz, R. *Scanning Probe Microscopy*; Springer-Verlag: Berlin Heidelberg, 2004; DOI: 10.1007/978-3-662-09801-1.
(30) Roth, B. J.; Sepulveda, N. G.; Wikswo, J. P. Using a magnetometer to image a two-dimensional current distribution. *J. Appl. Phys.* **1989**, *65*, 361−372.
(31) Fallarino, L.; Berger, A.; Binek, C. Magnetic field induced switching of the antiferromagnetic order parameter in thin films of magnetoelectric chromia. *Phys. Rev. B: Condens. Matter Mater. Phys.* **2015**, *91*, No. 054414.
(32) Al-Mahdawi, M.; Shiokawa, Y.; Pati, S. P.; Ye, S.; Nozaki, T.; Sahashi, M. Apparent critical behaviour of sputter-deposited magnetoelectric antiferromagnetic Cr2O3 films near Néel temperature. *J. Phys. D: Appl. Phys.* **2017**, *50*, 155004.
(33) Kosub, T. Ferromagnet-Free Magnetoelectric Thin Film Elements. Ph.D. thesis, Technischen Universität Chemnitz, 2017.
(34) Thöle, F.; Fechner, M.; Spaldin, N. A. First-principles calculation of the bulk magnetoelectric monopole density: Berry phase and Wannier function approaches. *Phys. Rev. B: Condens. Matter Mater. Phys.* **2016**, *93*, 195167.
(35) Meier, Q. N.; Fechner, M.; Nozaki, T.; Sahashi, M.; Salman, Z.; Prokscha, T.; Suter, A.; Schoenherr, P.; Lilienblum, M.; Borisov, P.; Dzyaloshinskii, I. E.; Fiebig, M.; Luetkens, H.; Spaldin, N. A. Search for the magnetic monopole at a magnetoelectric surface. *Phys. Rev. X* **2019**, *9*, No. 011011.
(36) Shull, C. G.; Smart, J. S. Detection of Antiferromagnetism by Neutron Diffraction. *Phys. Rev.* **1949**, *76*, 1256−1257.
(37) Sosnowska, I.; Neumaier, T. P.; Steichele, E. Spiral magnetic ordering in bismuth ferrite. *J. Phys. C: Solid State Phys.* **1982**, *15*, 4835−4846.
(38) Schreyer, A.; Schmitte, T.; Siebrecht, R.; Bödeker, P.; Zabel, H.; Lee, S. H.; Erwin, R. W.; Majkrzak, C. F.; Kwo, J.; Hong, M. Neutron scattering on magnetic thin films: Pushing the limits (invited). *J. Appl. Phys.* **2000**, *87*, 5443−5448.
(39) Nolting, F.; Scholl, A.; Stohr, J.; Seo, J. W.; Fompeyrine, J.; Siegwart, H.; Locquet, J. P.; Anders, S.; Luning, J.; Fullerton, E. E.; Toney, M. F.; Scheinfein, M. R.; Padmore, H. A. Direct observation of the alignment of ferromagnetic spins by antiferromagnetic spins. *Nature* **2000**, *405*, 767−769.
(40) Alders, D.; Tjeng, L. H.; Voogt, F. C.; Hibma, T.; Sawatzky, G. A.; Chen, C. T.; Vogel, J.; Sacchi, M.; Iacobucci, S. Temperature and thickness dependence of magnetic moments in NiO epitaxial films. *Phys. Rev. B: Condens. Matter Mater. Phys.* **1998**, *57*, 11623−11631.
(41) Kuiper, P.; Searle, B. G.; Rudolf, P.; Tjeng, L. H.; Chen, C. T. X-ray magnetic dichroism of antiferromagnet Fe_2O_3: The orientation of magnetic moments observed by Fe 2p x-ray absorption spectroscopy. *Phys. Rev. Lett.* **1993**, *70*, 1549−1552.
(42) Mertins, H.-C.; Oppeneer, P. M.; Kuneš, J.; Gaupp, A.; Abramsohn, D.; Schäfers, F. Observation of the X-Ray Magneto-Optical Voigt Effect. *Phys. Rev. Lett.* **2001**, *87*, No. 047401.
(43) Valencia, S.; Kleibert, A.; Gaupp, A.; Rusz, J.; Legut, D.; Bansmann, J.; Gudat, W.; Oppeneer, P. M. Quadratic X-Ray Magneto-Optical Effect upon Reflection in a Near-Normal-Incidence Configuration at the *M* Edges of *3d*-Transition Metals. *Phys. Rev. Lett.* **2010**, *104*, 187401.
(44) Saidl, V.; Němec, P.; Wadley, P.; Hills, V.; Campion, R. P.; Novák, V.; Edmonds, K. W.; Maccherozzi, F.; Dhesi, S. S.; Gallagher, B. L.; Trojánek, F.; Kuneš, J.; Železný, J.; Malý, P.; Jungwirth, T. Optical determination of the Néel vector in a CuMnAs thin-film antiferromagnet. *Nat. Photonics* **2017**, *11*, 91−96.

DOI: 10.1021/acs.nanolett.8b04681
Nano Lett. 2019, 19, 1682−1687